

DETAILED INVESTIGATION OF THE 4D PHASE-SPACE OF AN ION BEAM

H. R. Kremers[#], J.P.M. Beijers, S. Brandenburg, V. Mironov, S. Saminathan*

KVI, Groningen, The Netherlands

Abstract

A second order transfer matrix is calculated, which is used in the calculation of a 4D phase-space distribution of a 24.6 keV He¹⁺ beam. The calculated distribution matches a 4D phase-space distribution measured with the KVI pepper pot emittance meter. The pepper pot emittance meter is installed in the image plane of a dipole magnet acting as a charge-state analyser directly downstream the KVI AECR ion source. From the second order transfer matrix simple analytical equations are derived by retaining the terms for angular coefficients. These simple equations describe the main features of the phase-space correlations in the image plane. The equations show also that the subset of the 4D phase-space distribution, selected by one pepper pot aperture, results in multiple beam-lets. Due to this successful matrix modelling we conclude that the 4D phase-space distribution measured is fully determined by the ion-optical properties of the magnet.

INTRODUCTION

At KVI we have investigated the low transmission efficiency of the low-energy injection beam line of the superconducting cyclotron AGOR. For this investigation a pepper pot emittance meter [1] has been developed. With such an instrument the 4D phase space distribution was measured of a 24.6 keV He¹⁺ beam in the image plane of the dipole charge-state analyzing magnet of the AECR ion source. In the measured response distribution multiple beam-lets were seen. Using second order matrix calculations of the setup a method has been developed to describe the measured phase-space distribution in a simple way. In the section ‘transfer matrix’ the Taylor expansion into second order is presented which can be written as an second order matrix. In the section ‘simplification’ simple analytical expressions are derived which reproduce the main features of the correlations. In the section ‘measurements’ we shown that the simple expressions describe the distributions in the projections of the measured 4D phase-space.

TRANSFER MATRIX

For the determination of the second order matrix we use the COSY Infinity 9.1 [2] code. The code is based on the principle that Taylor expansion coefficients are calculated to describe the action of ion optical elements

on the phase-space coordinates in a curvilinear coordinate system. The code includes the technique of differential algebra in the numerical integrations, which permits the computation of Taylor expansions coefficients into arbitrary order. With the code a second order expression (see Eq. 1) is derived which maps the 4D state vector (x, x', y, y') of the beam from point A in an object plane to a position B in the image plane.

$$\begin{aligned} \theta_1 = & (\theta | x)x_0 + (\theta | x')x'_0 + (\theta | y)y_0 \\ & + (\theta | y')y'_0 + (\theta | xx)x_0^2 + (\theta | xx')x_0x'_0 \\ & + (\theta | x'x')x_0'^2 + (\theta | xy)x_0y_0 + (\theta | x'y)y_0' \\ & + (\theta | xy')x_0y'_0 + (\theta | x'y')x'_0y'_0 \\ & + (\theta | yy)y_0^2 + (\theta | yy')y_0y'_0 + (\theta | y'y')y_0'^2 \end{aligned} \quad (1)$$

In this expression the θ_1 can be replaced by the coordinate x_1, x'_1, y_1 and y'_1 in the image plane. The terms within the bracket are the expansion coefficients. The values of these coefficients are calculated with COSY Infinity 9.1 and are shown in Table 1. They depend on drift spaces, dipole geometry and fringe fields. The dimensions of the experimental setup and main features of the magnet are described elsewhere [3].

As initial conditions in the transformation, the ions start from a small point source (σ 2mm) in a virtual object plane under random angles r'_0 with the beam axis not exceeding 64 mrad. This angle r'_0 represents the initial transversal momentum of an ion.

$$r_0'^2 = x_0'^2 + y_0'^2 \quad (2) \quad E_t = \frac{1}{2} m r_0'^2 \quad (3)$$

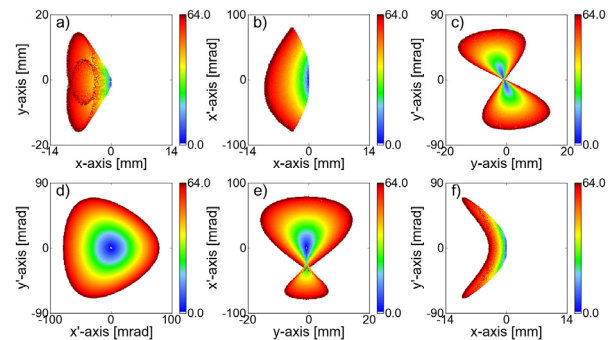


Figure 1: Calculated correlations of the initial transversal momentum r'_0 and the following combination of phase-space coordinates in the image plane: a) x-y, b) x-x', c) y-y', d) x'-y', e) y-x', e) x-y'. The colour code represents the initial transversal momentum r'_0 .

[#] email: kremers@kvi.nl

* present address: TRIUMF, 4004, Wesbrook Mall, Vancouver, CANADA

Table 1: Expansion coefficients of the overall transfer matrix in COSY Infinity notation with each individual significance in percentage of the contribution to the final value normalized to 1 mm and 64 mrad (spatial units in [m] and angular units in[rad]).

$\Theta_1 = x_1$	%	$\Theta_1 = x'_1$	%	$\Theta_1 = y_1$	%	$\Theta_1 = y'_1$	%	ID coeff
0.82648	-6.2	2.26816	3.7	0	0	0	0	(θ/x)
1.668E-06	0	1.20995	125.1	0	0	0	0	(θ/x')
0	0	0	0	-0.85078	-3.1	-1.258137	2.4	(θ/y)
0	0	0	0	9.100E-02	21.2	-1.040819	126	(θ/y')
-1.3220	0	-0.84624	0	0	0	0	0	(θ/x^2)
-2.0211	1	-1.6758	-0.2	0	0	0	0	(θ/xx')
-0.94047	28.9	-1.1015	-7.3	0	0	0	0	(θ/x'^2)
0	0	0	0	1.96766	0	-3.98394	0	(θ/xy)
0	0	0	0	3.85987	0.9	-3.84397	0.5	$(\theta/x'y)$
0	0	0	0	5.16242	1.2	5.65309	-0.7	(θ/xy')
0	0	0	0	5.34891	79.8	3.59906	-27.8	$(\theta/x'y')$
-3.35827	0	-5.66803	0	0	0	0	0	(θ/y^2)
-3.03125	1.5	-6.27946	-0.6	0	0	0	0	(θ/yy')
-2.43596	74.8	-3.12330	-20.7	0	0	0	0	(θ/y'^2)

These simple initial conditions describe in a general way the back projection of a simulated emittance described elsewhere [3]. This simulated emittance is the result of a LORENTZ3D transport-simulation where ions start from a simulated spatial distribution in a virtual extraction aperture of a ECR ion source.

The phase-space coordinates of 10^6 ions are transformed from the object plane to the image plane using Eq.1 which results in a calculated 4D phase-space distribution in the image plane. From this 4D phase-space distribution six correlations are visualized (see Fig. 1). In Fig. 1 the colour represents the value of the initial transversal momentum r'_0 of the ion. In Fig. 1a the correlation between r'_0 and the spatial phase-space coordinates in the image plane are shown. In Fig. 1b,1c the correlation is shown of r'_0 and the x - x' and y - y' phase-space coordinates. Figure 1d shows how the angular distribution is organized around the beam axis correlated to the initial transversal momentum.

SIMPLIFICATION

The second order equation Eq.1 is a simplified expression as a mono-energetic beam is assumed. The terms with $\Delta p/p$ are not printed. It is a reasonable assumption as the energy spread measured by Rodrigues et al. [4] is in the order of 14-24 eV/q with respect to an applied extraction voltage of 24.6 keV and the expansion coefficient $(x|p)$ which is 5.4mm / % $\Delta p/p$.

In order to better understand the six correlations visualized in Fig. 1, Eq.1 is simplified further and stripped from the terms which are not significant. The significance can be determined by normalizing the equation for a maximum in starting conditions which we have set on spatially 1 mm and angular 64 mrad. Given the small object size only the terms for the angular coordinates in Eq. 1 need to be retained. The resulting equations for the phase-space coordinates are then:

$$x_1 = (x | x' x') x'_0 x'_0 + (x | y' y') y'_0 y'_0 \quad (4)$$

$$x'_1 = (x' | x') x'_0 \quad (5)$$

$$y_1 = (y | y') y'_0 + (y | x' y') x'_0 y'_0 \quad (6)$$

$$y'_1 = (y' | y') y'_0 \quad (7)$$

Two main effects can be seen. The first effect is a correlation between x_1 coordinate in the image plane and the initial transversal velocity and the second effect is a cross correlation between x'_0 and y'_0 . The first effect can be seen after the introduction of a polar coordinate system where $x'_0 = r'_0 \cos \alpha$ and $y'_0 = r'_0 \sin \alpha$. After substitution of the polar coordinates in Eq.4 one finds relation Eq.8.

$$\frac{x_1}{r'^2_0} = (x | x' x') + ((x | y' y') - (x | x' x')) \sin^2 \alpha \quad (8)$$

In Eq.8 one can see that the ratio x_1/r'^2_0 is constant for α close to zero. Furthermore, $\sin^2 \alpha$ is always positive and the coefficients are negative (see Table.1). Therefore, all ions arrive in the image plane at a negative x_1 coordinate. (see Fig. 1a). This is caused by the fact that ions with larger initial transversal velocity have lower longitudinal velocity and consequently are bend over a larger angle than 110 degrees. Furthermore, if we substitute (5) and (7) in (4) a description of an ellipsoid in the x'_1 - y'_1 phase-space coordinates is found. The size of the ellipsoids increases as a function of x_1 . The major and minor axes of these ellipsoid are given by:

$$a = \sqrt{|x_1|} (x' | x') / \sqrt{(x | x' x')} \quad (9)$$

$$b = \sqrt{|x_1|} (y' | y') / \sqrt{(x | y' y')} \quad (10)$$

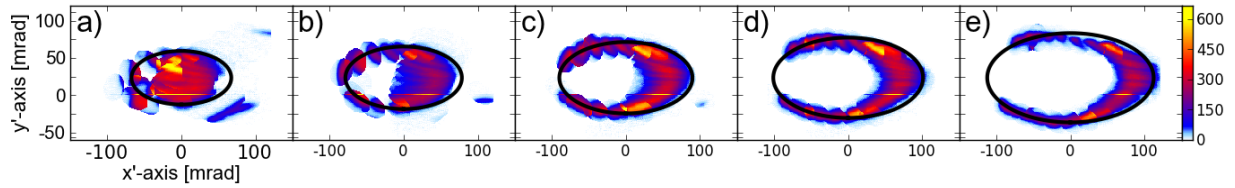


Figure 2: Measured sliced x' - y' projection as function of five scan positions: a) $x_1 = -2$ mm, b) $x_1 = -3.5$ mm, c) $x_1 = -5.0$ mm, d) $x_1 = -6.5$ mm, e) $x_1 = -8.0$ mm. Black lines are from Eq.5 and Eq.7 substituted in Eq.4.

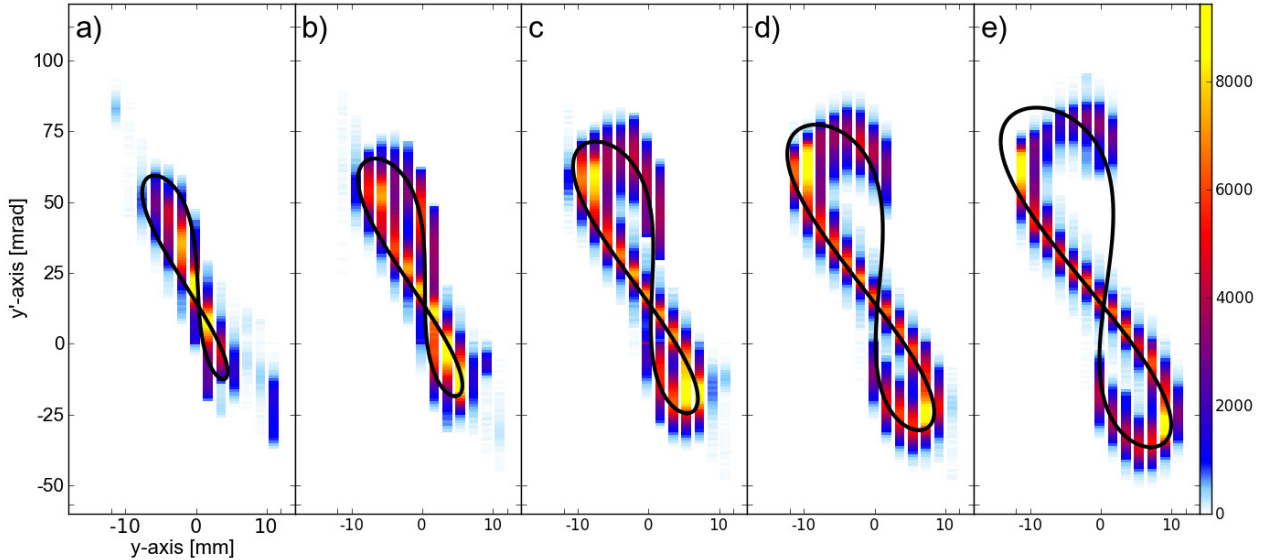


Figure 3: Measured sliced y' - y' projection at five different scan positions: a) $x_1 = -2$ mm, b) $x_1 = -3.5$ mm, c) $x_1 = -5.0$ mm, d) $x_1 = -6.5$ mm, e) $x_1 = -8.0$ mm. Black lines are from Eq.11 and Eq.7 in polar coordinates.

The second effect of the cross correlation can be seen in Eq.11 which results when Eq.6 is rewritten in polar coordinates. A closer look at Eq.11 shows that the term with ' $\sin(2\alpha)$ ' generates the 'figure eight' distribution (see Fig. 1c).

$$y_1 = (y | y')r'_0 \sin \alpha + (y | x'y')r_0'^2 \cdot \frac{1}{2} \sin 2\alpha \quad (11)$$

The coefficient $(y|x'y')$ describes the 'strength' of the 'figure eight' in the distributions. This term is also responsible for the multiple beam-lets as for some values of y_1 one finds four different values of y' .

MEASUREMENTS

The two effects described in section above are clearly visible in the projections of the measured 4D phase-space distribution of the 24.6 keV He^{1+} beam. First, effect as describe earlier, can be observed in the measured x' - y' projection (see Fig. 2) at five different x_1 positions. Each distribution separately is described by an ellipsoid derived from the Taylor expansion with values for major and minor axis derived from the expansion coefficients.

The second effect identified as a cross correlation between x' and y' is also observed in the measurements. In Fig. 3 the measured y' - y' projection of the 4D phase-

space distribution is shown for five x_1 positions. The measured distributions are well described with the curves defined by Eq.7 and Eq.11.

CONCLUSIONS

The measured 4D phase-space distribution of an ion beam is successfully calculated with the help of a second order transfer map developed with COSY Infinity 9.1. The beam characteristics behind the magnet are fully determined by the ion-optical properties of the magnet. Further, the structure of the phase-space distribution is clarified with a simple model extracted from the second order transfer map.

ACKNOWLEDGMENT

This work is part of the research program of the "Stichting voor Fundamenteel Onderzoek der Materie" (FOM) with financial support from the "Nederlandse organisatie voor Wetenschappelijk Onderzoek" (NOW). It is supported by the University of Groningen and by "Gesellschaft für Schwerionenforschung GmbH" (GSI), Darmstadt, Germany. We acknowledge the financial support of the European Union Seventh Framework Program FP7/2007- 2013 under Grant Agreement n° 262010 - ENSAR.

REFERENCES

- [1] Kremers, H.R., J.P.M. Beijers, and S. Brandenburg, A Versatile Emittance Meter and Profile Monitor, in DIPAC07. May 2007: Venice, Italy. p. 195-197.
- [2] Makino, K. and M. Berz, COSY INFINITY Version 9. Nuclear Instruments & Methods in Physics Research Section a-Accelerators Spectrometers Detectors and Associated Equipment, 2006. 558(1): p. 346-350.
- [3] Saminathan, S., et al., Optimization of a charge-state analyzer for electron cyclotron resonance ion source beams. Review of Scientific Instruments. 83(7): p. 073305 (6 pp.)-073305 (6 pp.).
- [4] Rodrigues, G., et al., Effect of source tuning parameters on the plasma potential of heavy ions in the 18 GHz high temperature superconducting electron cyclotron resonance ion source. The Review of scientific instruments. 83(3): p. 033301.